Structural Investigation of Encapsulated Fluoride in Polyhedral Oligomeric Silsesquioxane Cages Using Ion Mobility Mass Spectrometry and Molecular Mechanics

Stanley E. Anderson,[‡] Dena J. Bodzin,[†] Timothy S. Haddad,[§] Jerry A. Boatz,[||] Joseph M. Mabry,[||] Connie Mitchell,[†] and Michael T. Bowers*[,†]

Department of Chemistry & Biochemistry, University of California, Santa Barbara, California 93106, Department of Chemistry, Westmont College, Santa Barbara, California 93108, ERC Inc., Air Force Research Laboratory, 10 East Saturn Boulevard, Building 8451, Edwards Air Force Base, California 93524-7680

Received January 7, 2008. Revised Manuscript Received April 22, 2008

A new series of encapsulated fluoride polyhedral oligomeric silsesquioxane (POSS) materials, $[(CH_3)_4N^+][F^-@(R_8Si_8O_{12})]$, where R = vinyl, phenyl, styrenyl, trifluoropropyl, nonafluorohexyl, or tridecafluorooctyl, were synthesized by the reaction of tetramethylammonium fluoride with the $R_8Si_8O_{12}$ POSS in tetrahydrofuran. Encapsulation of the fluoride was confirmed with ^{19}F and ^{29}Si NMR spectroscopy. Ion mobility and molecular modeling methods were used to investigate the gas phase conformational properties of these POSS. Theoretical calculations demonstrate that the binding energy of fluoride to the interior of the POSS cage ranges from 70 to 270 kcal/mol as a function of substituent. Sodiated positive ions of the form $H^+[F^-@R_8T_8]Na^+$ (T = $SiO_{3/2}$, R = styrenyl, phenyl, and vinyl) were examined by MALDI; ESI was used to study the negative ions $F^-@R_8T_8$ (R = styrenyl, phenyl, vinyl, trifluoropropyl, and nonafluorohexyl). The ion mobilities of these species were measured and used to calculate collision cross sections. These cross sections were compared to X-ray crystal structures and theoretical cross sections obtained from molecular mechanics and dynamics calculations. Experimental cross sections were consistent with all of the known X-ray crystal structures (styrenyl, vinyl, and phenyl POSS species). The experimental cross sections also agreed with the calculated cross sections for each species. As a result of the compact nature of the POSS cages, each sample had only one stable conformation, and only one low-energy family of structures was found for each set of sample calculations.

Introduction

In the field of materials science, much current research focuses on the ability to enhance properties of materials for increased performance and environmental robustness. One approach to developing better materials is to create inorganic/organic composite materials in which inorganic building blocks are incorporated into organic polymers. Polyhedral oligomeric silsesquioxanes (POSS) are one type of hybrid inorganic/organic material of the form $(RSiO_{3/2})_n$, abbreviated R_nT_n, where organic substituents (R_n) are attached to a silicon−oxygen cage.[1] The most common POSS cage is the R_8T_8, a molecule with a cubic array of silicon atoms and bridging oxygen atoms with eight R groups at the vertexes of the cube; other cages with well-defined geometries include n = 6, 10, 12, 14, 16, and 18.[2–4] When these Si−O cage structures are incorporated into organic polymers, exciting possibilities for the development of new materials are often realized,[5–16] with properties superior to the original organic polymer. For example, the low surface energy properties of fluorinated POSS compounds have been used to augment both fluorinated and nonfluorinated polymers.[17–20]

* Corresponding author. Phone: 805-893-2893. E-mail: bowers@chem.ucsb.edu.
‡ Westmont College.
† University of California.
§ ERC Inc.
|| Air Force Research Laboratory.

(1) Voronkov, M. G.; Lavrentyev, V. I. *Top. Curr. Chem.* **1982**, *102*, 199–236.
(2) Agaskar, P. A. *Inorg. Chem.* **1991**, *30*, 2707–2708.
(3) Agaskar, P. A.; Klemperer, W. G. *Inorg. Chim. Acta* **1995**, *229*, 355–364.
(4) Rikowski, E.; Marsmann, H. C. *Polyhedron* **1997**, *16*, 3357–3361.
(5) Pielichowski, K.; Njuguna, J.; Janowski, B.; Pielichowski, J. *Adv. Polym. Sci.* **2006**, *201*, 225–296.
(6) Baney, R. H.; Itoh, M.; Sakakibara, A.; Suzuki, T. *Chem. Rev.* **1995**, *95*, 1409–1430.
(7) Lichtenhan, J. D. *Comments Inorg. Chem.* **1995**, *17*, 115–130.
(8) Lichtenhan, J. D. *Polymeric Materials Encyclopedia*; CRC Press: New York, 1996.
(9) Li, G. Z.; Wang, L. C.; Ni, H. L.; Pittman, C. U. *J. Inorg. Organomet. Polym.* **2001**, *11*, 123–154.
(10) Phillips, S. H.; Haddad, T. S.; Tomczak, S. J. *Curr. Opin. Solid State Mater. Sci.* **2004**, *8*, 21–29.
(11) Li, G. Z.; Pittman, C. U., Jr. Containing Metals and Metal-like Elements. *Macromolecules* **2005**, *4*, 79−131.
(12) Joshi, M.; Butola, B. S. *J. Macromol. Sci., Polym. Rev.* **2004**, *C44*, 389–410.
(13) Harrison, P. G. *J. Organomet. Chem.* **1997**, *542*, 141–183.
(14) Abe, Y.; Gunji, T. *Prog. Polym. Sci.* **2004**, *29*, 149–182.
(15) Provatas, A.; Matisons, J. G. *Trends Polym. Sci. (Cambridge, U.K.)* **1997**, *5*, 327–332.
(16) Kannan, R. Y.; Salacinski, H. J.; Butler, P. E.; Seifalian, A. M. *Acc. Chem. Res.* **2005**, *38*, 879–884.
(17) Iacono, S. T.; Budy, S. M.; Mabry, J. M.; Smith, D. W., Jr *Macromolecules* **2007**, *40*, 9517–9522.
(18) Koh, K.; Sugiyama, S.; Morinaga, T.; Ohno, K.; Tsujii, Y.; Fukuda, T.; Yamahiro, M.; Iijima, T.; Oikawa, H.; Watanabe, K.; Miyashita, T. *Macromolecules* **2005**, *38*, 1264–1270.
(19) Dodiuk, H.; Rios, P. F.; Dotan, A.; Kenig, S. *Polym. Adv. Technol.* **2007**, *18*, 746–750.

10.1021/cm800058z CCC: $40.75 © 2008 American Chemical Society
Published on Web 06/12/2008

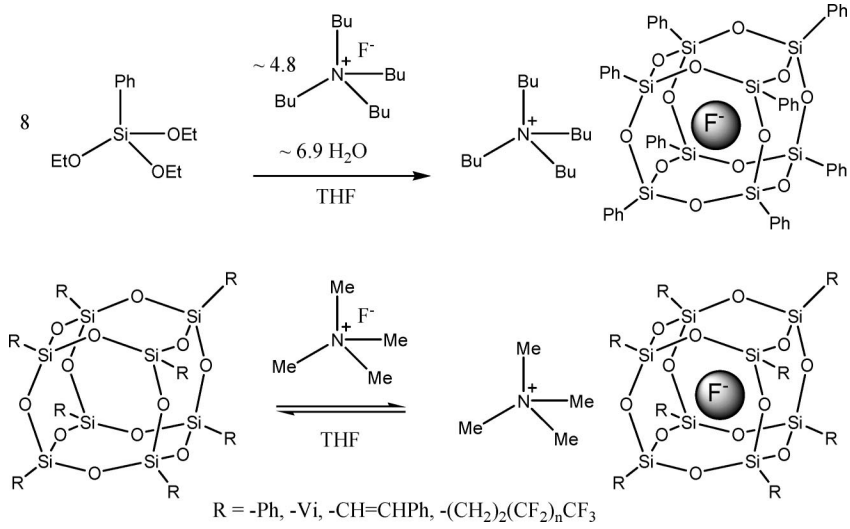

Figure 1. Synthesis and structure of F^-@Phenyl$_8$Si$_8$O$_{12}$. The upper reaction is the literature synthesis from ref 33. The lower reaction (this work) is more complicated that a simple insertion reaction and involves the breaking and reforming of Si−O bonds.

Many POSS monomers have been successfully characterized using MALDI techniques[21,22] in conjunction with ion mobility mass spectrometry (IMMS).[23–25] The POSS cages have good ionization efficiencies due to electronegative atoms or π-electron density in the R-groups and readily bind protons or alkali metal cations to give positive ions. Fragmentation of the cage may occur at high laser powers, but this has not been enough of a factor to prevent observation of a strong molecular ion peak. Bulky alkyl R-groups seem to inhibit the formation of positive ions, and signals for such POSS species are rarely seen.

Extending the study of POSS systems from monomers to polymers and oligomers relies on our ability to generate large ions in the gas phase without fragmentation. Ion mobility studies coupled with molecular dynamics modeling of other types of large polymers,[21,26,27] including DNA[28,29] and proteins,[30] have shown great success. However, there are only a few papers reporting mass spectra of POSS polymers.[31] Larger POSS oligomers may have lower ionization efficiencies than the monomers, most likely due to decreased charge density, because POSS cages are efficient in delocalizing electron density. The oligomers may also have an increased tendency to fragment. Our group has been successful in characterizing two oligomer systems, the POSS propylmethacrylates and siloxanes, but only up to systems with three POSS cages.[28,32] The intensity of the molecular ion peak generally decreases with increasing oligomer size to the point that it becomes impossible to obtain ion mobility data. To facilitate the observation of higher POSS oligomers by mass spectrometric methods, it has been necessary to develop new strategies that will enhance the ionization efficiency of these compounds.

Methods for increasing the ionization efficiency of these POSS materials must begin with the synthesis of these molecules. Both acid- and base-catalyzed methods have proved fruitful in creating many new molecules with a variety of R-groups, but often in relatively low yield.[1] Bassindale and co-workers[33–36] have succeeded not only in increasing the POSS yield dramatically by using tetrabutylammonium fluoride (TBAF) under scarce-water hydrolysis conditions as a catalyst but also in synthesizing a new class of POSS materials in which a fluoride ion is trapped in the center of a POSS cage, denoted F^-@R_8T_8 (see upper reaction Figure 1). They have demonstrated incorporation of fluoride into the cage using NMR chemical shifts and have obtained crystal structures for R = vinyl, phenyl, and *p*-tolyl, where the F^- ion is clearly in the center of the cage. The fluoride ion results in only a very slight change in the Si−O distances

(20) Tuteja, A.; Choi, W.; Ma, M.; Mabry, J. M.; Mazzella, S. A.; Rutledge, G. C.; McKinley, G. H.; Cohen, R. E. *Science (Washington, DC)* **2007**, *318*, 1618–1622.
(21) Baker, E. S.; Gidden, J.; Fee, D. P.; Kemper, P. R.; Anderson, S. E.; Bowers, M. T. *Int. J. Mass Spectrom.* **2003**, *227*, 205–216.
(22) Baker, E. S.; Gidden, J.; Anderson, S. E.; Haddad, T. S.; Bowers, M. T. *Nano Lett.* **2004**, *4*, 779–785.
(23) Bowers, M. T.; Kemper, P. R.; von Helden, G.; van Koppen, P. A. M. *Science* **1993**, *260*, 1446–1451.
(24) von Helden, G.; Hsu, M.-T.; Kemper, P. R.; Bowers, M. T. *J. Chem. Phys.* **1991**, *95*, 3835–3837.
(25) Wyttenbach, T.; Bowers, M. T. *Top. Curr. Chem.* **2003**, *225*, 207–232.
(26) Gidden, J.; Jackson, A. T.; Scrivens, J. H.; Bowers, M. T. *Int. J. Mass Spectrom.* **1999**, *188*, 121–130.
(27) Gidden, J.; Bowers, M. T.; Jackson, A. T.; Scrivens, J. H. *J. Am. Soc. Mass Spectrom.* **2002**, *13*, 499–505.
(28) Anderson, S. E.; Baker, E. S.; Mitchell, C.; Haddad, T. S.; Bowers, M. T. *Chem. Mater.* **2005**, *17*, 2537–2545.
(29) Gabelica, V.; Baker, E. S.; Teulade-Fichou, M. P.; De Pauw, E.; Bowers, M. T. *J. Am. Chem. Soc.* **2007**, *129*, 895–904.
(30) Baumketner, A.; Bernstein, S. L.; Wyttenbach, T.; Bitan, G.; Teplow, D. B.; Bowers, M. T.; Shea, J. E. *Protein Sci.* **2006**, *15*, 420–428.
(31) Wallace, W. E.; Guttman, C. M.; Antonucci, J. M. *J. Am. Soc. Mass Spectrom.* **1999**, *10*, 224–230.
(32) Anderson, S. E.; Mitchell, C.; Haddad, T. S.; Vij, A.; Schwab, J. J.; Bowers, M. T. *Chem. Mater.* **2006**, *18*, 1490–1497.
(33) Bassindale, A. R.; Liu, Z.; MacKinnon, I. A.; Taylor, P. G.; Yang, Y.; Light, M. E.; Horton, P. N.; Hursthouse, M. B. *Dalton Trans.* **2003**, 2945–2949.
(34) Bassindale, A. R.; Chen, H.; Liu, Z.; MacKinnon, I. A.; Parker, D. J.; Taylor, P. G.; Yang, Y.; Light, M. E.; Horton, P. N.; Hursthouse, M. B. *J. Organomet. Chem.* **2004**, *689*, 3287–3300.
(35) Bassindale, A. R.; Parker, D. J.; Pourny, M.; Taylor, P. G.; Horton, P. N.; Hursthouse, M. B. *Organometallics* **2004**, *23*, 4400–4405.
(36) Bassindale, A. R.; Pourny, M.; Taylor, P. G.; Hursthouse, M. B.; Light, M. E. *Angew. Chem., Int. Ed.* **2003**, *42*, 3488–3490.

and cage bond angles from structures where the central fluoride is absent.

The electronic structure, stabilities, and NMR spectra of F^-@POSS species have been studied using high level DFT calculations in attempts to understand the mechanism of encapsulation.[37–39] In particular, the stability of the F^-@POSS cage depends on the nature of the organic capping groups. When the R group is a highly delocalized π-system such as phenyl,[40] the HOMO and LUMO are outside of the cage primarily centered on the organic ligands. This predicts the center of the cage will have a more positive charge, stabilizing the fluoride structure. Conversely, when R is an electron donating alkyl group, [41,42] the HOMO is associated primarily with the cage atoms, predicting in a more negative charge on the cage. This would destabilize the fluoride structure. In fact, attempts to synthesize fluoride salts of alkyl-substituted POSS have failed. Clearly additional theoretical calculations are needed to understand the stability of the F^-@POSS for a range of R groups.

A new series of F^-@POSS species with a Me_4N^+ counterion have been synthesized from preformed $R_8Si_8O_{12}$ cages and tetramethylammonium fluoride (see lower reaction in Figure 1). These materials have been characterized by ^{29}Si, ^{19}F NMR spectroscopy, ion mobility mass spectrometry, and molecular modeling techniques. The R groups that yielded isolable F^-@POSS structures include phenyl, vinyl, styrenyl, trifluoropropyl, nonafluorohexyl, and tridecafluorooctyl. Each of these R groups demonstrates electron-withdrawing properties, accounting for the stabilization of the interior fluoride ion as predicted.

Incorporation of the fluoride into these compounds suggests a tool to study higher molecular weight POSS-containing oligomers. If even a single POSS cage within an oligomer were able to incorporate fluoride, this would increase its ionization efficiency. If several of the POSS units in the oligomer incorporated fluoride ions, it would greatly increase ionization efficiency as well as reduce the mass to charge ratio of the ion, resulting in a sample that would be easier to study by mass spectrometric methods. Here we describe in detail our initial studies of F^- bound in the interior of the POSS cage and demonstrate the effectiveness of IMMS for studying these systems.

Materials and Methods

General POSS Synthesis Procedures. POSS materials used for this study were either purchased from Hybrid Plastics ($Methyl_8T_8$, $Vinyl_8T_8$, $Phenyl_8T_8$, $Phenyl_{12}T_{12}$, $isoButyl_8T_8$, $CycloHexyl_8T_8$) or else synthesized according to the literature procedures[43–48] ($Ethyl_8T_8$, $TrifluoroPropyl_8T_8$, $NonafluoroHexyl_8T_8$, $TridecafluoroOctyl_8T_8$, $Styrenyl_8T_8$, $isoButyl_7(Styryl)T_8$). Two sources of tetramethylammonium fluoride (TMAF) were used. No significant differences were noted between reactions using commercially available material (Aldrich, used as received) and high purity anhydrous material generously provided by Prof. K.O. Christe.[49] Tetrahydrofuran (THF) was dried through an activated alumina column,[50] freeze−pump−thawed three times to remove any oxygen, and stored under an inert nitrogen atmosphere in a dry box. THF-d_8 (Cambridge) used in NMR experiments was dried over sodium benzophenone.

Synthesis of F^-@POSS Salts. All syntheses were carried out in the same manner: 200 mg of the parent POSS cage along with 1 mol equiv of TMAF was placed into 10 mL of anhydrous THF and stirred for 16 h. A sample synthesis is as follows: In a 25 mL flask, 200 mg (0.194 mmol) of $Phenyl_8T_8$ and 18 mg (0.19 mmole) of TMAF were suspended in THF and stirred for 16 h. The cloudy suspension became translucent after 3 h. This was filtered through Celite, and the solvent was removed under vacuum to give a 92% yield of F^-@POSS salt. This synthesis worked well for POSS cages substituted with electron withdrawing groups: vinyl ($Si-CH=CH_2$), phenyl ($Si-C_6H_5$), styrenyl ($Si-CH=CHC_6H_5$), trifluoropropyl ($Si-CH_2CH_2CF_3$), nonafluorohexyl ($Si-CH_2CH_2CF_2CF_2CF_2CF_3$), and tridecafluorooctyl ($Si-CH_2CH_2CF_2CF_2CF_2CF_2CF_2CF_3$). Isolated yields were all over 90%. It failed to produce any F^-@POSS product for cages substituted with the electron donating groups, methyl, ethyl, isobutyl, or cyclohexyl. In these cases, only unreacted starting material was recovered. Complex mixtures of products were obtained using POSS cages with both types of substituents such as $isoButyl_7(Styryl)T_8$ and $Phenyl_7(ethylnorbornene)T_8$. Products were characterized by ^{29}Si and ^{19}F NMR, before and after reaction with TMAF. ^{29}Si and ^{19}F NMR spectra were referenced to either external tetramethylsilane or $CFCl_3$ at 0 ppm. The ^{19}Si NMR spectra show changes in the environments of the silicon atoms, and the ^{19}F NMR show an additional fluoride present in each sample after reaction with TMAF. The details of this characterization are summarized in the Supporting Information.

Ion Mobility/Mass Spectrometry. High-resolution mass spectra were acquired using a PE Sciex QStar quadrapole/time-of-flight tandem mass spectrometer with a nano-ESI source. Two different home-built instruments were used for the ion mobility mass spectrometry experiments on these compounds. The components and operation of these instruments have been previously published,[28,32,51] and the details will not be repeated here. In each case, the instrument can be used to generate a mass spectrum, where a range of m/z is detected, or an arrival time distribution (ATD), where a specific m/z is detected as a function of time.

MALDI. To examine positive ions, a MALDI-TOF equipped with an ion mobility drift cell was used.[28,32] The matrix was 2,5-dihydroxybenzoic acid (DHB) with THF as the solvent. Approximately 60 μL of DHB (100 mg/mL), 40 μL of POSS (1 mg/mL), and 8 μL of NaI (saturated solution) were mixed and applied to the sample target. A nitrogen laser ($\lambda = 337$ nm, 12 mW power)

(37) Hossain, D.; Pittman, C. U., Jr.; Saebo, S.; Hagelberg, F. *J. Phys. Chem. C* **2007**, *111*, 6199–6206.
(38) Park, S. S.; Xiao, C.; Hagelberg, F.; Hossain, D.; Pittman, C. U., Jr.; Saebo, S. *J. Phys. Chem. A* **2004**, *108*, 11260–11272.
(39) Tossell, J. A. *J. Phys. Chem. C* **2007**, *111*, 3584–3590.
(40) Lin, T.; He, C.; Xiao, Y. *J. Phys. Chem. B* **2003**, *107*, 13788–13792.
(41) Xiang, K. H.; Pandey, R.; Pernisz, U. C.; Freeman, C. *J. Phys. Chem. B* **1998**, *102*, 8704–8711.
(42) Franco, R.; Kandalam, A. K.; Pandey, R.; Pernisz, U. C. *J. Phys. Chem. B* **2002**, *106*, 1709–1713.
(43) Poliskie, G. M.; Haddad, T. S.; Blanski, R. L.; Gleason, K. K. *Thermochim. Acta* **2005**, *438*, 116–125.
(44) Mabry, J. M.; Iacono, S. T.; Viers, B. D. *Angew. Chem., Int. Ed.*, **2008**, *4*, 4137–4140.
(45) Haddad, T. S.; Viers, B. D.; Phillips, S. H. *J. Inorg. Organomet. Polym.* **2001**, *11*, 155–164.
(46) Lichtenhan, J. D.; Schwab, J. J. ; An, Y.-Z.; Reinerth, W.; Carr, M. J.; Feher, F. J.; Terroba, R.; Liu, Q. U.S. Patent 6972312, 2005.
(47) Iacono, S. T.; Vij, A.; Grabow, W.; Smith, D.W., Jr.; Mabry, J. M. *Chem. Commun.* **2007**, *499*, 4992–4994.
(48) Feher, F. J.; Soulivong, D.; Eklund, A. G.; Wyndham, K. D. *Chem. Commun.* **1997**, 1185–1186.
(49) Christe, K. O.; Wilson, W. W.; Wilson, R. D.; Bau, R.; Feng, J. A. *J. Am. Chem. Soc.* **1990**, *112*, 7619–7625.
(50) Pangborn, A. B.; Giardello, M. A.; Grubbs, R. H.; Rosen, R. K.; Timmers, F. J. *Organometallics* **1996**, *15*, 1518–1520.
(51) Wyttenbach, T.; Kemper, P. R.; Bowers, M. T. *Int. J. Mass Spectrom.* **2001**, *212*, 13–23.

was used to ionize the sample in the ion source. The ions were guided out of the source with 9 kV of extraction voltage, and sent through a 1-m flight tube. The ions were then reflected and redirected to a detector, resulting in a high-resolution mass spectrum of the ions generated at the source. To perform ion mobility measurements, the reflecting lenses were switched off, and the ions continued out of the flight tube to a mass gate. There, mass-selected ions were injected into a 20-cm glass drift cell filled with ~1.5 Torr of helium gas. The ions drifted through the cell under the influence of a weak electric field, passed through a quadrupole mass filter, and were detected.

ESI. The instrument used to analyze the negative POSS samples was a nano-ESI, also equipped with an ion mobility cell.[51] Approximately 7 μL of POSS solution (~0.1 mg/mL in THF) was loaded into a metalized glass needle. A voltage was applied between the needle and the instrument, spraying the solution out of the needle, through a capillary and into an ion funnel. The ions were then injected into a 4.5 cm drift cell filled with ~5 Torr of helium gas. Again, the ions were pulled through with a weak electric field. After exiting the cell, the ions were mass analyzed by a quadrupole mass filter and detected.

Data Analysis. For each of these instruments, a timing sequence is initiated when the pulse of ions is generated for injection into the drift cell. The time it takes for these ions to reach the detector, t_A, is the sum of the time spent in the drift cell, t_d, and the time spent out of the drift cell, t_o. The amount of time that is required for an ion to drift through a cell filled with helium depends on how many collisions the ion has with the buffer gas, which in turn depends on the effective mobility of the ion. These collisions, along with the electric field across the cell, result in a constant drift velocity v_d

$$v_d = KE = K_o E \frac{760}{P} \frac{T}{273.16} \quad (1)$$

where K is the mobility of the ion at temperature T and pressure p and K_o is the reduced mobility. Equation 1 can be rewritten in terms of the arrival time

$$t_A = \frac{l^2}{K_o} \frac{1}{760} \frac{273}{T} \left(\frac{P}{V}\right) + t_o \quad (2)$$

where l is the cell length and V is the voltage across the cell. A plot of t_A versus p/V yields a straight line with a slope proportional to $1/K_o$ and an intercept of t_o. Once K_o is known, it is straightforward to find the cross section σ from eq 3

$$\sigma = \frac{3q}{16NK_o}\left(\frac{2\pi}{\mu K_b T}\right)^{1/2} \quad (3)$$

where q is the charge on the ion, N is the number density of the gas in the cell, μ is the ion-He reduced mass, and k_b is Boltzmann's constant.[52]

Theoretical Modeling. We carried out molecular mechanics/molecular dynamics (MM/MD) calculations using the AMBER 7 and 8 suites of programs[53–55] to obtain low-energy structures, and an annealing protocol that utilizes repeated cycles of high temperature heating, cooling, and energy minimization. The annealing protocol typically heats structures to 1400 K for 10 ps and then cools exponentially for 30 ps to 50 K before energy minimization. Cations were restrained using a built-in AMBER distance restraint so that they did not "dissociate" at high temperature. At least 100 candidate structures were used to generate a diagnostic graph of calculated cross sections versus relative energy. To model POSS materials, we developed AMBER parameters for Si from the ab initio calculations of Sun and Rigby[56,57] that were originally designed to provide force field parameters for polysiloxanes. Our parameter database was updated using recent crystal structure data[33,58] which give more accurate Si−O and Si−C distances and which reproduce experimental cross sections. We used HyperChem[59] to build starting structures for AMBER and to visually inspect the calculated minimum energy structures. Charges were calculated by the standard RESP protocol.

A modified projection model[23,60] was used to calculate accurate cross sections for systems with masses below about 1500 amu. For systems above about 1500 amu this method underestimates the true cross section, due to the occurrence of multiple ion-He encounters during collisions. Between 1500 and 5000 amu a trajectory model is utilized that incorporates a Lennard-Jones interaction portenial.[61] It is our experience that this model can, at times, overestimate the cross section, but usually gives more reliable values than the projection model in this size range. For larger systems the Lennard-Jones potential is replaced by a hard sphere potential that generally gives reliable results.[62]

Electronic Structure Calculations. Density functional theory (DFT) calculations[63] utilizing the B3LYP hybrid functional[64–66] and the 6-31G* basis set,[67–72] denoted as B3LYP/6-31G*, were carried out using the Gaussian 03[73] and GAMESS[59,74] quantum chemistry software packages. The latter program was the primary computational tool because of its ability to run efficiently in parallel

(52) Mason, E. A.; McDaniel, E. W. *Transport properties of ions in gases*; Wiley: New York, 1988.

(53) Case, D. A.; Pearlman, D. A.; Caldwell, J. W.; Cheatham, T. E., III; Wang, J.; Ross, W. S.; Simmerling, C. L.; Darden, T. A.; Merz, K. M.; Stanton, R. V.; Cheng, A. L.; Vincent, J. J.; Crowley, M.; Tsui, V.; Gohlke, H.; Radmer, R. J.; Duan, Y.; Pitera, J.; Massova, I.; Seibel, G. L.; Singh, U. C.; Weiner, P. K.; Kollman, P. A. AMBER 7, University of California: San Francisco, 2002.

(54) Case, D. A.; Darden, T. A.; Cheatham T. E., III; Simmerling, C. L.; Wang, J.; Duke, R. E.; Luo, R.; Merz, K. M. ; Wang, B.; Pearlman, D. A.; Crowley, M. ; Brozell, S.; Tsui, V.; Gohlke, H.; Mongan, J.; Hornak, V.; Cui, G.; Beroza, P.; Schafmeister, C.; Caldwell, J. W.; Ross, W. S.; Kollman, P. A. AMBER 8, University of California: San Francisco, 2004.

(55) Case, D. A.; Pearlman, D. A.; Caldwell, J. W.; Cheatham, T. E., III; Ross, W. S.; Simmerling, C.; Darden, T.; Merz, K. M.; Stanton, R. V.; Cheng, A.; Vincent, J. J.; Crowley, M.; Tsui, V.; Radmer, R.; Duan, Y.; Pitera, J.; Massova, I.; Seibel, G. L.; Singh, U. C.; Weiner, P.; Kollman, P. A. AMBER 6, University of California: San Francisco, 1999.

(56) Sun, H. *Macromolecules* **1995**, *28*, 701–712.

(57) Sun, H.; Rigby, D. *Spectrochim. Acta, Part A* **1997**, *53*, 1301–1323.

(58) Itami, Y.; Marciniec, B.; Kubicki, M. *Chem.—Eur. J.* **2004**, *10*, 1239–1248.

(59) Gordon, M. S., Schmidt, M. W., Theory and Applications of Computational Chemistry, the first forty years. In ed. Dykstra, C. E., Frenking, G., Kim, K. S., Scuseria, G. E., Eds.; Elsevier: Amsterdam, 2005.

(60) von Helden, G.; Wyttenbach, T.; Bowers, M. T. *Int. J. Mass Spectrom. Ion Processes* **1995**, *146*, 349–364.

(61) Mesleh, M. F.; Hunter, J. M.; Shvartsburg, A. A.; Schatz, G. C.; Jarrold, M. F. *J. Phys. Chem.* **1996**, *100*, 16082–16086.

(62) Shvartsburg, A. A.; Jarrold, M. F. *Chem. Phys. Lett.* **1996**, *261*, 86–91.

(63) Kohn, W.; Becke, A. D.; Parr, R. G. *J. Phys. Chem.* **1996**, *100*, 12974–12980.

(64) Stephens, P. J.; Devlin, F. J.; Chabalowski, C. F.; Frisch, M. J. *J. Phys. Chem.* **1994**, *98*, 11623–11627.

(65) Becke, A. D. *J. Chem. Phys.* **1993**, *98*, 5648–5652.

(66) Becke, A. D. *Phys. Rev. A* **1988**, *38*, 3098–3100.

(67) Ditchfield, R.; Hehre, W. J.; Pople, J. A. *J. Chem. Phys.* **1971**, *54*, 724.

(68) Hehre, W. J.; Ditchfield, R.; Pople, J. A. *J. Chem. Phys.* **1972**, *56*, 2257.

(69) Dill, J. D.; Pople, J. A. *J. Chem. Phys.* **1975**, *62*, 2921–2923.

(70) Francl, M. M.; Pietro, W. J.; Hehre, W. J.; Binkley, J. S.; Gordon, M. S.; Defrees, D. J.; Pople, J. A. *J. Chem. Phys.* **1982**, *77*, 3654–3665.

(71) Harihara, Pc; Pople, J. A. *Theor. Chim. Acta* **1973**, *28*, 213–222.

(72) Gordon, M. S. *Chem. Phys. Lett.* **1980**, *76*, 163–168.

using hundreds of processors. The geometry of each species was fully optimized and verified as a local minimum on the ground-state potential energy surface via diagonalization of the matrix of energy second derivatives with respect to nuclear coordinates, that is, the Hessian matrix. Selected species were reoptimized using the more flexible 6-311++G(d,p) basis set[71,75–77] (B3LYP/6-311++G(d,p)). Finally, relative energies were refined via DFT and second order perturbation theory (MP2, also known as MBPT(2)[78–81]) single-point energy calculations using the 6-311++G(2df) basis set[75–77] at the B3LYP/6-31G* geometries, denoted as B3LYP/6-311++G(2df)//B3LYP/6-31G* and MP2/6-311++G(2df)//B3LYP/6-31G*, respectively.

Results and Discussion

The reaction in THF (dried through an alumina column) of TMAF with R_8T_8 POSS cages containing eight electron withdrawing groups leads to near quantitative conversion to a salt in which the fluoride ion is trapped within the POSS cage (Figure 1). ^{29}Si and ^{19}F NMR spectra of the products are consistent with a single pure compound being formed, and the chemical shifts are comparable to those reported by Bassindale et al. for tetra-*butyl*-ammonium POSS fluoride salts (see Figure 2a−d). ^{29}Si NMR shows that addition of the fluoride to the cage results in about a 3 ppm shift to lower frequency. The reaction is successful for R = phenyl, vinyl, styrenyl, trifluoropropyl, nonafluorohexyl, and tridecafluorooctyl POSS derivatives. All attempts to incorporate fluoride into the electron-donating alkyl POSS cages of $(ethyl)_8T_8$, $(cyclohexyl)_8T_8$, and $(i\text{-}Butyl)_8T_8$ failed, with only unreacted starting material recovered; no observable signal was found in the ^{19}F NMR spectra, and ^{29}Si spectra revealed only T_8 starting material.

The reaction is more complex than a simple addition of fluoride into the cage. Although it is theoretically possible for the fluoride to insert directly into the cage[38] it is more likely that the fluoride reacts at the silicon and catalyzes the exchange of silicon groups among cages; it is also possible that this reaction is assisted by traces of water. Figure 2e shows the ^{29}Si NMR spectrum obtained when $[(CH_3)_4N^+][F^-@(Phenyl_8Si_8O_{12})]$ and $[(CH_3)_4N^+][F^-@(Vinyl_8Si_8O_{12})]$ are mixed together in THF-d_8. Prior to mixing, these molecules are stable with no change to their spectra over time. The appearance of several signals between those of the pure starting materials indicates that many compounds are being generated with mixed phenyl and vinyl groups. Further evidence for the complexity of this reaction is given in Figure 2f. Addition of 2 equiv of $(CH_3)_4N^+F^-$ to $(Phenyl_8Si_8O_{12})$ and $(Vinyl_8Si_8O_{12})$ in THF-d_8 generates a complex ^{29}Si NMR spectrum that is consistent with many isomers being generated. In fact there are 22 possible isomers for a T_8 cage with two R groups. Rikowski and Marsmann have shown that cage scrambling of T8's can be catalyzed by various inorganic salts, including sodium fluoride, in acetone and acetonitrile.[4] An attempt to follow the formation of $[(CH_3)_4N^+][F^-@(Vinyl_8Si_8O_{12})]$ by ^{19}F NMR spectroscopy revealed only one resonance. No intermediates were observable, although the intensity of the single product peak increased as the reaction progressed and the Me_4NF was taken into solution by the $Vinyl_8Si_8O_{12}$.

Mass spectra and ion mobility for most of the synthesized POSS fluoride salts were also obtained and will be discussed in turn. The calculated and experimental cross sections for each negative ion of the form $F^-@R_8T_8$ are given in Table 1, and the equivalent measurements of the sodiated species, $H^+[F^-@R_8T_8]Na^+$, are given in Table 2. It should be emphasized that the MALDI MS experiment results in protonation of the POSS fluoride species with an H^+ derived from the matrix material to give a neutral. The presence of a large excess of NaI ensures that this neutral POSS species becomes sodiated. In addition, some of the in situ reactions of POSS with TMAF were carried out using wet THF that resulted in reaction and rearrangement of the POSS cages (vide infra). Such products cannot be isolated since the observed ions are generated in the gas phase via ESI and MALDI ionization processes. Protonated and otherwise cationized species were identified by their masses.

$F^-@Phenyl_8T_8$. The synthesis of $F^-@Phenyl_8T_8$ from $Phenyl_8T_8$ and TMAF yields a single well-characterized product. However, a related synthesis of $F^-@Phenyl_7$-(ethylnorbornene)T_8 gives a mixture of products in which there are chemical shifts indicative of three fluoride environments (−26.27, −26.30, and −26.34 ppm) plus another chemical shift which exactly matches pure $F-@Phenyl_8T_8$ (−26.50 ppm). This implies that the fluoride ion causes cage rearrangement to the more stable symmetrically substituted parent. The NMR spectrum for $F^-@Phenyl_8T_8$ gives a single ^{19}F chemical shift consistent with trapped fluoride. A $Phenyl_8T_8$ and $Phenyl_{12}T_{12}$ mixture reacted with TMAF gives exclusively the $F^-@Phenyl_8T_8$ product as shown both by NMR and mass spectroscopy (see Figure 3). The multiple peaks commencing at *m/z* 1051 reveal an isotope distribution which corresponds exactly with the calculated ^{13}C theoretical distribution. A single peak ATD is observed with a width

(73) Frisch, M. J.; Trucks, G. W.; Schlegel, H. B.; Scuseria, G. E.; Robb, M. A.; Cheeseman, J. R.; Montgomery, J., J. A.; Vreven, T.; Kudin, K. N. ; Burant, J. C.; Millam, J. M.; Iyengar, S. S.; Tomasi, J.; Barone, V.; Mennucci, B.; Cossi, M.; Scalmani, G.; Rega, N.; Petersson, G. A.; Nakatsuji, H.; Hada, M.; Ehara, M.; Toyota, K.; Fukuda, R.; Hasegawa, J.; Ishida, M.; Nakajima, T.; Honda, Y. ; Kitao, O.; Nakai, H.; Klene, M.; Li, X.; Knox, J. E.; Hratchian, H. P.; Cross, J. B.; Bakken, V.; Adamo, C.; Jaramillo, J.; Gomperts, R.; Stratmann, R. E.; Yazyev, O. ; Austin, A. J.; Cammi, R.; Pomelli, C.; Ochterski, J. W.; Ayala, P. Y.; Morokuma, K.; Voth, G. A.; Salvador, P.; Dannenberg, J. J.; Zakrzewski, V. G.; Dapprich, S.; Daniels, A. D.; Strain, M. C.; Farkas, O.; Malick, D. K.; Rabuck, A. D.; Raghavachari, K.; Foresman, J. B.; Ortiz, J. V.; Cui, Q.; Baboul, A. G.; Clifford, S.; Cioslowski, J.; Stefanov, B. B.; Liu, G.; Liashenko, A.; Piskorz, P.; Komaromi, I.; Martin, R. L.; Fox, D. J.; Keith, T.; Al-Laham, M. A.; Peng, C. Y.; Nanayakkara, A.; Challacombe, M.; Gill, P. M. W.; Johnson, B.; Chen, W.; Wong, M. W.; Gonzalez, C.; Pople, J. A. *Gaussian 03*; Gaussian, Inc.: Wallingford, 2004.
(74) Schmidt, M. W.; Baldridge, K. K.; Boatz, J. A.; Elbert, S. T.; Gordon, M. S.; Jensen, J. H.; Koseki, S.; Matsunaga, N.; Nguyen, K. A.; Su, S. J.; Windus, T. L.; Dupuis, M.; Montgomery, J. A. *J. Comput. Chem.* **1993**, *14*, 1347–1363.
(75) Krishnan, R.; Binkley, J. S.; Seeger, R.; Pople, J. A. *J. Chem. Phys.* **1980**, *72*, 650–654.
(76) Clark, T.; Chandrasekhar, J.; Spitznagel, G. W.; Schleyer, P. V. *J. Comput. Chem.* **1983**, *4*, 294–301.
(77) Frisch, M. J.; Pople, J. A.; Binkley, J. S. *J. Chem. Phys.* **1984**, *80*, 3265–3269.
(78) Moller, C.; Plesset, M. S. *Phys. Rev.* **1934**, *46*, 618–622.
(79) Pople, J. A.; Binkley, J. S.; Seeger, R. *Int. J. Quantum Chem.* **1976**, 1–19.
(80) Frisch, M. J.; Headgordon, M.; Pople, J. A. *Chem. Phys. Lett.* **1990**, *166*, 275–280.
(81) Bartlett, R. J.; Silver, D. M. *Int. J. Quantum Chem. Symp.* **1975**, *9*, 183–198.

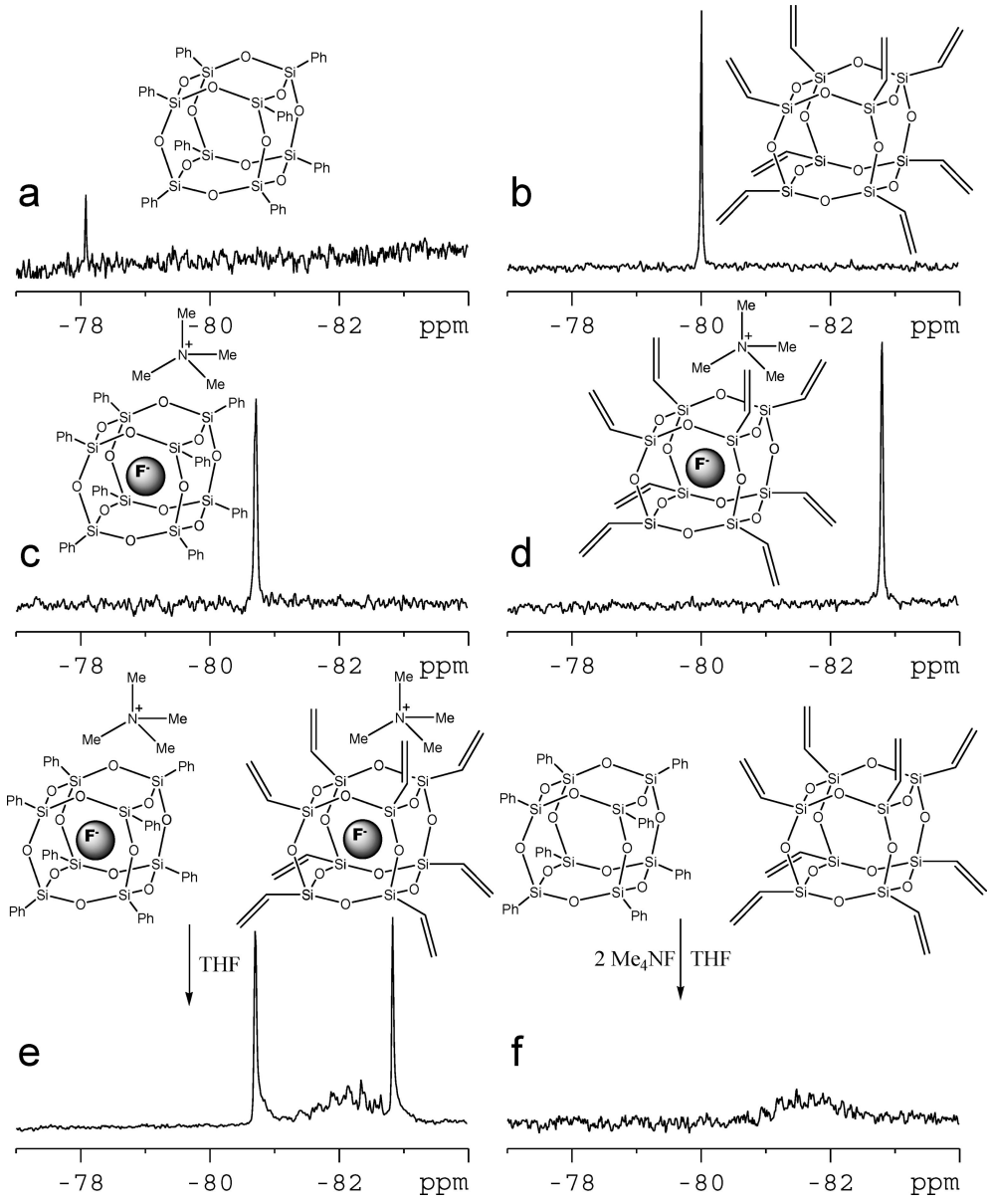

Figure 2. ^{29}Si NMR spectra of several POSS materials: (a) $Phenyl_8Si_8O_{12}$; (b) $Vinyl_8Si_8O_{12}$; (c) $[Me_4N^+][F^-@Phenyl_8Si_8O_{12}]$; and (d) $[Me_4N^+][F^-@Vinyl_8Si_8O_{12}]$. (e) Spectrum obtained from mixing $F^-@Vinyl_8Si_8O_{12}$ and $F^-@Phenyl_8Si_8O_{12}$ in THF; (f) spectrum obtained from mixing Me_4NF with equivalent amounts of $Vinyl_8Si_8O_{12}$ and $Phenyl_8Si_8O_{12}$ in THF.

Table 1. Collision Cross Sections (Å^2) of the Negative POSS Fluoride Ions[a]

species	mass	X-ray[b] cross section	ESI cross section	theory
$F^-@Ph_8T_8$	1051	260	268	260
$F^-@Vi_8T_8$	651	168	165	167
$F^-@Vi_{10}T_{10}$	809		189	190
$F^-@Vi_{12}T_{12}$	967		210	212, 214[c]
$F^-@Sty_8T_8$	1259	343	346	343
$F^-@i\text{-}Bu_6St_2T_8$	983		258	258[d]
$F^-@i\text{-}Bu_5St_3T_8$	1029		272	271[d]
$F^-@i\text{-}Bu_4St_4T_8$	1075		283	284[d]
$F^-@Fpr_8T_8$	1211	261[e]	251	256
$F^-@Fhex_8T_8$	2411	350[e]	376	368

[a] Vi = vinyl; Ph = phenyl; Sty = styrenyl; i-Bu = i-butyl; Fhex = $(CF_3)(CF_2)_3(CH_2)_2$; Fpr = $CF_3CH_2CH_2$; St = styryl, $T_8 = Si_8O_{12}$. [b] Calculated value for the neutral species. [c] Values correspond to two possible isomers. [d] Values identical for all possible isomers within experimental error. [e] Reference 37.

consistent with a single species with an experimental cross section of 268 Å^2. Molecular modeling predicts a single family of structures with a calculated cross section of 260 Å^2. The positive ion, which corresponds in mass to $H^+[F^-@Phenyl_8T_8]Na^+$, was examined by MALDI and also shows a single ATD feature (Figure 4) with an experimental cross section of 254 Å^2. This compares with a theoretical cross section of 257 Å^2 for this sodiated species. We cannot experimentally determine the precise location of the proton. Two possible sites are protonation of an edge oxygen or recombination with the $@F^-$ to give a @HF. Unfortunately both species have nearly identical cross sections and hence

Table 2. Collision Cross Sections (Å^2) of the Sodiated POSS Fluorides[a]

Species	Mass	X-ray[b]	MALDI (Na^+) cross section	Theory (Na^+)
$H^+[F^-@Sty_8T_8]Na^+$	1284		321	325
$H^+[F^-@Ph_8T_8]Na^+$	1075	263	254	257
$H^+[F^-@Vi_8T_8]Na^+$	674	168	165	167
$H^+[F^-@Fpr_8T_8]Na^+$	1235		218	216

[a] Vi = vinyl; Ph = phenyl; Sty = styrenyl; i_Bu = i-butyl; Fpr = fluoropropyl; $T_8 = Si_8O_{12}$. [b] Calculated value for the neutral species.

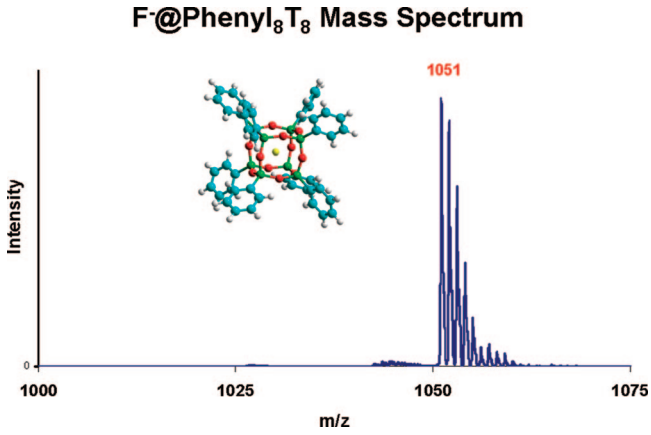

Figure 3. ESI mass spectrum of F^-@Phenyl$_8$T$_8$. The ^{13}C isotope distribution commencing with m/z = 1051 corresponds to the theoretically expected distribution.

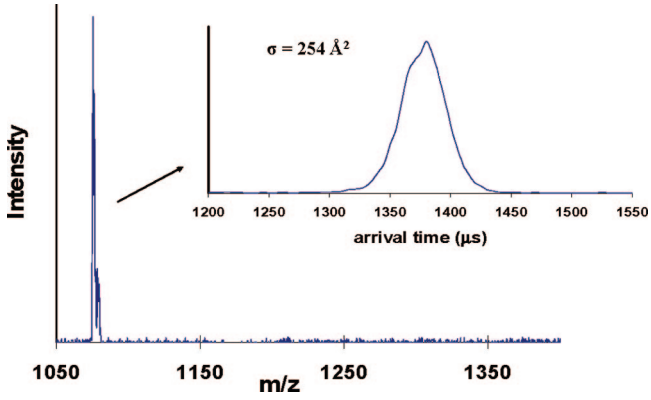

Figure 4. MALDI mass spectrum and ATD (inset) of HF@Phenyl$_8$T$_8$Na$^+$.

cannot be distinguished using ion mobility. Thermodynamics strongly favors the @F^- protonation however. The recombination of a proton with F- is exoergic by 255.3 kcal/mol.[82] While the proton affinity for the Si_8O_{12} cage is not known but is probably less than CO_2 (128 kcal/mol), it is definitely less than H_2O (173.0 kcal/mol).[83] Hence in all probability, protonation of the cage will almost instantaneously lead to neutralization of @F^- with formation of @HF.

If a mixture of Ph_8T_8 and $Ph_{12}T_{12}$ is reacted in situ with TMAF in "wet" THF, a much more complex mass spectrum is observed (see Figure 5). Instead of the exclusive fluoride species observed in Figure 3, a number of oxo species can be asssigned to the observed masses which arise from degradation of the cage by complex reaction with fluoride in the presence of substantial water. Figure 6 gives the structures of several of these ions and the calculated cross sections. The mechanism for formation of these species is unknown but must involve a preliminary step of either F^- or OH^- atacking an edge of the POSS cage to open it up, followed by insertion of a Ph-SiO_2^- fragment and ring closure to reform a larger cage. The mass spectrum shows that this is consistent with the pattern of oxo species formed

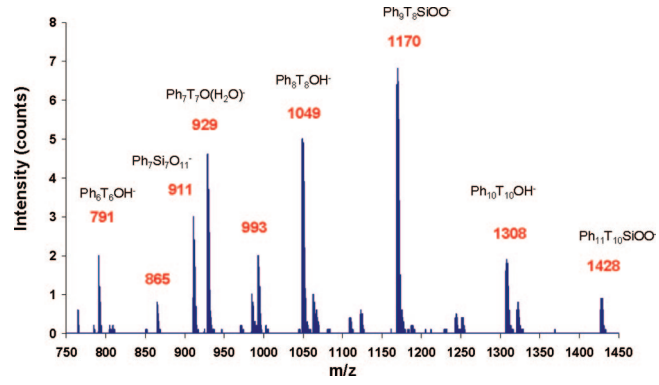

Figure 5. ESI mass spectrum of oxo species derived from Ph_8T_8, $Ph_{12}T_{12}$ and Me_4NF in wet THF.

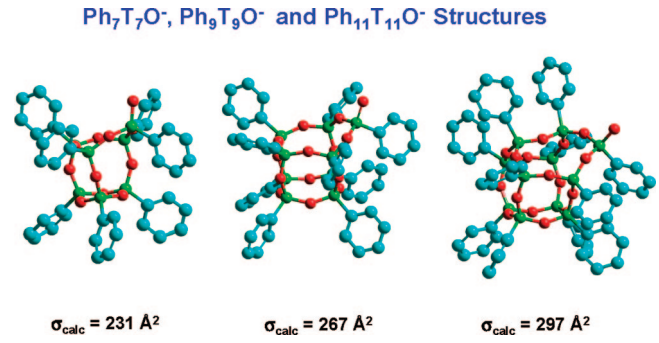

Figure 6. $Ph_7T_7O^-$, $Ph_9T_9O^-$ and $Ph_{11}T_{11}O^-$ structures derived from Ph_8T_8, $Ph_{12}T_{12}$, and Me_4NF in wet THF. Silicon atoms are green, O is red, C atoms are blue, and H atoms are omitted.

from each of the Ph_nT_n parents. Species which correspond to $-OH^-$ products are possibly analogous to the encapsulated fluoride ions; the isoelectronic hydroxide ion inserts itself into the center of the cage to give a species with nearly identical cross section to the parent.

F^-@Vinyl$_8$T$_8$ and F^-@Vinyl$_n$T$_n$. Synthesis of F^-@Vinyl$_8$T$_8$ from Vinyl$_8$T$_8$ and TMAF under nearly dry conditions gave a single product by ^{29}Si and ^{19}F NMR spectroscopy and mass spectrometry, the ESI mass spectrum being similar to Figure 3 centered on m/z 651. A single peak ATD is observed with a width consistent with a single species with an experimental cross section of 166 Å^2. Molecular modeling predicts a single family of structures with a calculated cross section of 167 Å^2. The MALDI generated positive ion, corresponding in mass to $H^+[F^-$@Vinyl$_8$-T$_8$]Na$^+$, shows a single ATD feature with an experimental cross section of 165 Å^2 in good agreement with a theoretical cross section of 167 Å^2. Again thermodynamics indicates recombination of H^+ with @F^- to form a @HF species.

The in situ reaction of a cage mixture of vinyl T_8, T_{10}, T_{12}, and T_{14} with Me_4NF in wet THF gives a mixture of products and it appears that the F^- anion was trapped inside all the various cage sizes. We did not observe isomerization of the larger cages to T_8 on the time scale of our experiment. A complex ESI mass spectrum (Figure 7) was observed showing the F^-@Vinyl$_n$T$_n$ negative ions where n = 8, 10, 12, and 14. The experimental cross sections of the fluoride species up to n = 12 (the n = 14 ATD intensity was too small to make arrival time measurements) are given in Table 1 and are in very close agreement with the theoretical values. Other peaks (e.g., m/z 721 and 878) correspond to the oxo

(82) Lias, S. G.; Bartmess, J. E.; Liebman, J. F.; Holmes, J. L.; Levin, R. D.; Mallard, W. G.; Lide, D. R. *J. Phys. Chem. Ref. Data* **1988**, *17* (Suppl. 1), 1–59.
(83) Aue, D. H.; Bowers, M. T. In *Gas Phase Ion Chemistry*; Bowers, M. T., Ed.; Academic Press: New York, 1979; Vol. 2, pp 1−52.

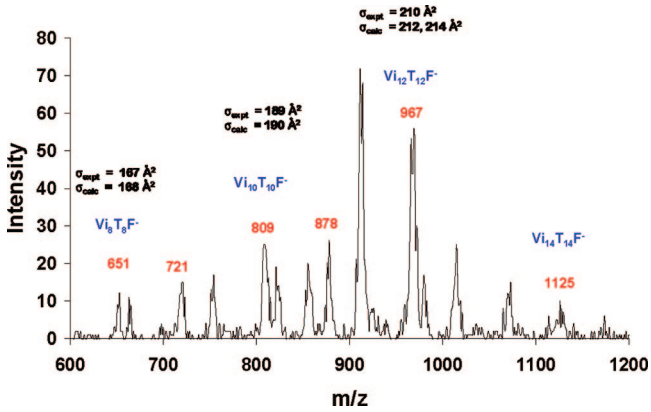

Figure 7. ESI mass spectrum of fluoride species derived from Vi_nT_n, Me_4NF, and wet THF.

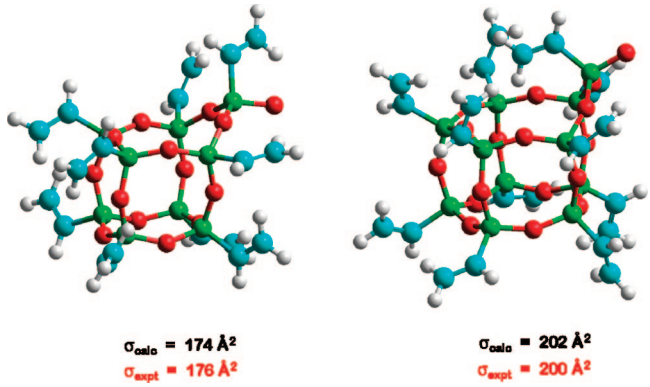

Figure 8. $Vi_9T_9O^-$ and $Vi_{11}T_{11}O^-$ structures derived from Vi_nT_n, Me_4NF and wet THF. Silicon atoms are green, O atoms are red, C atoms are blue, and H atoms are white.

species shown in Figure 8 with the formulas $Vi_9T_9O^-$ and $Vi_{11}T_{11}O^-$ based on the agreement of measured and modeled cross sections.

Calculations at the B3LYP/6-311++G(2df)//B3LYP/6-31G* and MP2/6-311++G(2df)//B3LYP/6-31G* levels predict the binding energy of the fluoride ion in the V_8T_8 cage to be −63 and −77 kcal/mol, respectively, which is quite large and accounts for the thermodynamic stability of such species. If the fluoride ion were bound on a face of the T_8 cage the binding energy of −37 kcal/mol is still considerable but significantly smaller, explaining the preference for encapsulation. MALDI ionization produces species in the TOF spectrum consistent with the formula $H^+[F^-@Vi_8T_8]$ M^+. If a proton adds to $F^-@Vi_8T_8$ giving a neutral $HF@Vi_8T_8$ and binding a M^+ cation, subsequent formation of either the Li^+ or Na^+ cationized species gives binding energies of −47 and −30 kcal/mol, respectively, at the MP2/6-311++G(2df)//B3LYP/6-31G* level. An encapsulated neutral species $HF@Vi_8T_8$ alone without a cation is not predicted to be stable. These results are summarized in Table 3 and pictorially in Figure 9.

To test the effect of possible matrix anions forming ion clusters to give the neutral species $T_mH_m \cdot M_nCl_n$, (m = 6, 8, 10; n = 1, 2, 4; M = Na^+, Li^+), the binding energies of these clusters are listed in Table 4. The M_nCl_n clusters are about 30−50 kcal/mol less stable than the cationized species but could still be formed. This would reduce the total ion current because of the POSS cages that would exist as neutral species in the gas phase instead of as ions. The effect of cage size (except for T_6) and cation (except for K^+) is minimal on these cluster binding energies and is not a factor for the R_8T_8 species studied because the positive ions used were consistently Li^+ or Na^+.

Table 3. MP2 and DFT Stabilization Energies for POSS Fluorides[a]

Species[b]	ΔE^c B3LYP/ 6-31G*	ΔE^d B3LYP/ 6-311++G(2df)	ΔE^e MP2/ 6-311++G(2df)
$F^-@(CF_3)_8T_8$ [f]	−170	−120	−270
fa-$(CF_3)_8T_8F^-$ [f]	−154	−102	−297
$F^-@(CH_3)_8T_8$ [f]	−112	−57	−70
$F^-@Vi_8T_8$ [f]	−119	−63	−77
fa-$Vi_8T_8F^-$ [f]	−80	−26	−37
$HF@Vi_8T_8$ [f]	+12	+29	+19
endo-$Vi_8T_8(OH)F^-$ [g]	−22	−11	−11
$HF@Vi_8T_8Na^+$ [h]	−40	−15	−30[i]
$HF@Vi_8T_8Li^+$ [h]	−59	−32	−47[i]
$[HF@Vi_8T_8]NaCl$ [j]	−8	15	40
$[HF@Vi_8T_8]LiCl$[j]	−12	12	−4
$F^-@[CF_3CH_2)_2]_8T_8$ [f]	−171		

[a] Vi = vinyl; $T_8 = Si_8O_{12}$. All structures computed at the B3LYP/6-31G* level. All binding energies include B3LYP/6-31G* zero point vibrational energy corrections (scaled by 0.9806; see Scott, A.P., Radom, L. *J. Phys. Chem.* **1996**, *100*, 16502.) [b] All optimized structures have F^- or HF body-centered unless specifically designated fa = "face". [c] B3LYP/6-31G*//B3LYP/6-31G * level of theory. [d] B3LYP/6-311++G(2df)//B3LYP/6-31G * level of theory. [e] MP2/6-311++G(2df)//B3LYP/6-31G * level of theory. Core orbitals were frozen in the MP2 calculation unless otherwise noted. [f] Binding energy $\Delta E = E(HF/F^-$ − POSS) − E(POSS) − $E(HF/F^-)$. [g] Additional isomer. [h] Binding energy $\Delta E = E(HF$ − POSS− $Li^+/Na^+)$ − E(POSS) − E(HF) − $E(Li^+/Na^+)$. [i] Core orbitals were included in MP2 calculation. [j] Binding energy $\Delta E = E$(HF − POSS − NaCl/LiCl) − E(POSS) − E(HF) − E(NaCl/LiCl).

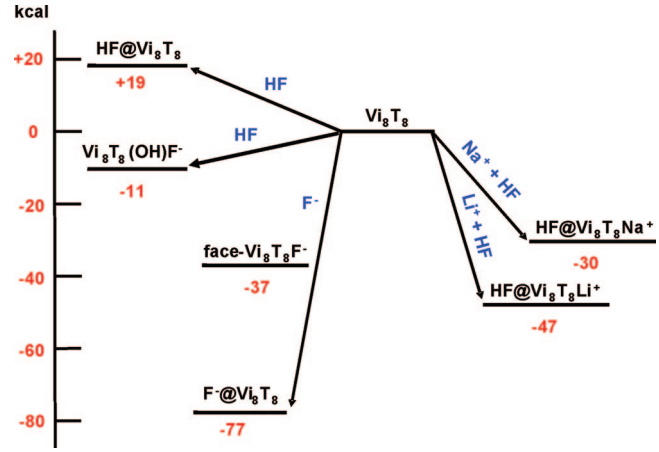

Figure 9. MP2 stabilization energies for Vi_8T_8 fluoride species.

Table 4. Neutral $T_mH_m \cdot M_nCl_n$ POSS Cluster Binding Energies (kcal/mol) as a Function of Cage Size[a]

species[b,c]	LiCl	Li_2Cl_2	Li_4Cl_4	NaCl	Na_2Cl_2	Na_4Cl_4	KCl
T_6H_6	−42.7			−14.7			+35
T_8H_8	−13.5	−11.2	−10.0	−10.1	−7.9	−7.2	1.3
$T_{10}H_{10}$	−15.2			−9.7			+11.1

[a] H = hydrogen; $T_8 = Si_8O_{12}$. [b] Binding energy, $\Delta E = E$(neutral parent) + $E(X_nCl_n)$ − $E(X_nCl_n$ cluster), where n = 1, 2, 4. [c] 6-311G* basis set with B3LYP functional; full energy minimization.

$F^-@Styenryl_8T_8$. The MALDI mass spectrum of the $Styrenyl_8T_8$ fluoride salt is shown in Figure 10. The mass spectrum corresponds to a sodiated ion in which the fluoride species is protonated to give either encapsulated HF or possibly protonated edge oxygen. The single peak in the ATD gives an experimental cross section of 321Å^2, which corresponds closely to the theoretical value of 325 Å^2. Again

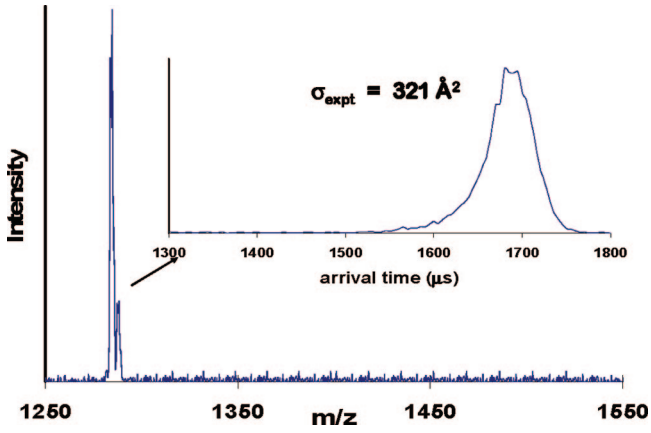

Figure 10. MALDI mass spectrum and ATD (inset) of fluoride species derived from sodiated HF@Styrenyl$_8$T$_8$.

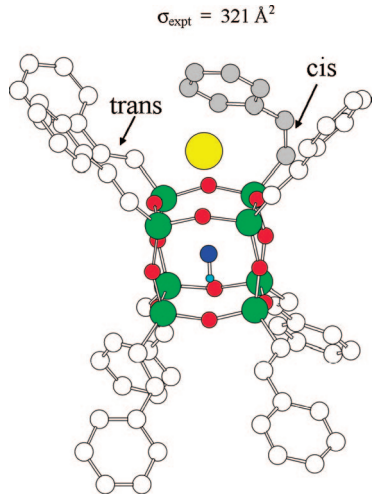

Figure 11. Structure of sodiated HF@Styrenyl$_8$T$_8$ ion. $\sigma_{expt} = 321$ Å^2 and $\sigma_{calcd} = 325$ Å^2.

we cannot experimentally distinguish various protonated structures since calculations give nearly identical cross sections. However, as mentioned earlier, the high proton affinity of F^- supports encapsulated HF and such species are stable based on our calculations.

The positive ion cross sections are consistent with one or two styrenyl groups having isomerized (Figure 11 shows one possible structure with HF@) from trans to cis to give a structure smaller than the all trans structure ($\sigma_{calcd} = 343$ Å^2). This explanation is consistent with previous mass spectrometry and ion mobility studies on the sodiated Styrenyl$_8$T$_8$ species that yielded a complex ATD corresponding to families of paired styrenyl groups and minor features corresponding to "cis isomers".[21,22] The cis structure cannot be an artifact of the synthesis, as the change would have been detectable by the NMR characterization, but it may be a result of activation of the double bond in the trans styrenyl group during the MALDI process. The fact that the all-trans species was not observed suggests the single cis isomer is more stable.

In contrast, the negative ion F^-@Styrenyl$_8$T$_8$, examined by ESI gives experimental and theoretical cross sections of 346 and 343 Å^2, respectively. It is clear that the all trans styrenyl species is dominant in the negative ion spectrum, no isomerization having occurred.

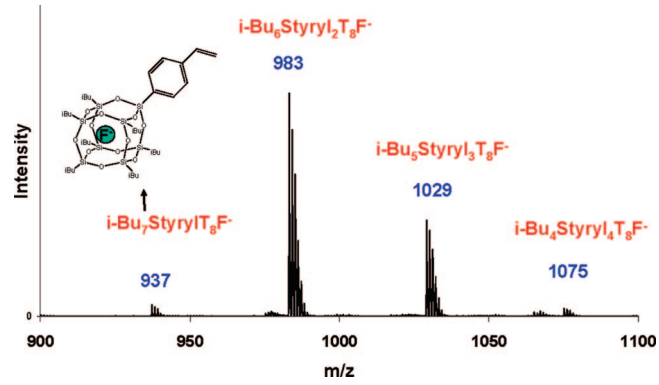

Figure 12. ESI mass spectrum of fluoride species derived from (i-Bu)$_7$(C$_6$H$_5$CH=CH$_2$)T$_8$. Silicon scrambling has occurred.

F^-@(i-Butyl)$_7$(Styryl)T$_8$. The ESI mass spectrum for the F^-@(i-Butyl)$_7$(Styryl)T$_8$ negative ion and other species related to the parent ion is given in Figure 12. The only reasonable explanation for these additional products is that in the presence of TMAF, the parent structure undergoes complex cage opning and rearrangement which scrambles the silicons and therefore the i-butyl and styryl groups. This is consistent with the ^{19}F NMR spectrum which shows at least six environments for the fluoride ion with chemical shifts between −24.5 and −26.3 ppm. Four of these are clearly identifiable in Figure 12. ATDs were measured for the most intense peaks and the cross sections from experiment and theory are in close agreement and are listed in Table 1.

F^-@Trifluoropropyl$_8$T$_8$. The ESI mass spectrum for the F^-@Trifluoropropyl$_8$T$_8$ species has a single peak at 1211 mass units corresponding to the parent ion. The experimental cross section from the ESI ATD is 251 Å^2, in good agreement with the calculated cross section of 256 Å^2. Using coordinates from a recent X-ray crystal structure[17] gives a calculated cross section of 261 Å^2, slightly larger than what is seen in the gas phase. This difference can be attributed to the way that the trifluoropropyl groups are constrained via nonbonded interactions or packing in the crystal.

A trifluoropropyl group differs from the previous phenyl, vinyl and styrenyl structures described above in that no extended π system is present. However, the CF_3 component of this R-group is strongly electron-withdrawing, which makes the cage more positively charged and thus facilitates incorporation of a fluoride ion. DFT calculations were used to study the electronic structure of $[CF_3(CH_2)_2]_8T_8$ and $(CF_3)_8T_8$ as well as the F^-@POSS species. The latter show a large F^- binding energy of −171 kcal/mol. The electron densities of the HOMO (molecular orbital 300) and LUMO (molecular orbital 301) are shown in Figure 13. Examination of the frontier orbitals in the vicinity of the HOMO and LUMO has indicated that the orbitals are primarily centered on the $CF_3(CH_2)_2$ groups rather than on the POSS cage. This is similar to the electronic structures of the previous ligands with extended π systems, where the cage has a net positive charge. It is not surprising that POSS cages with similar electronic structures incorporate fluoride in a similar manner to give stable products. In contrast, calculations on a POSS cage capped with methyl groups, Methyl$_8$T$_8$, show that the electron density is increased on the cage and F^-@Methyl$_8$T$_8$

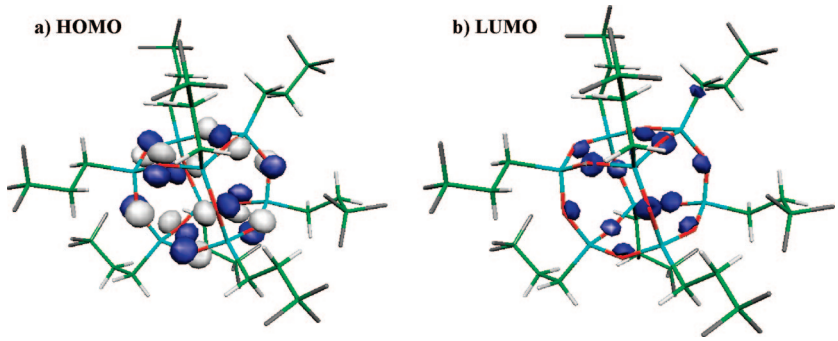

Figure 13. (a) HOMO of $[(CF_3(CH_2)_2]_8T_8$ comprised of cage oxygen lone pairs. (b) LUMO of $[(CF_3(CH_2)_2]_8T_8$ comprised of cage oxygen antibonding σ^* orbitals. Frontier orbitals are primarily centered on R group.

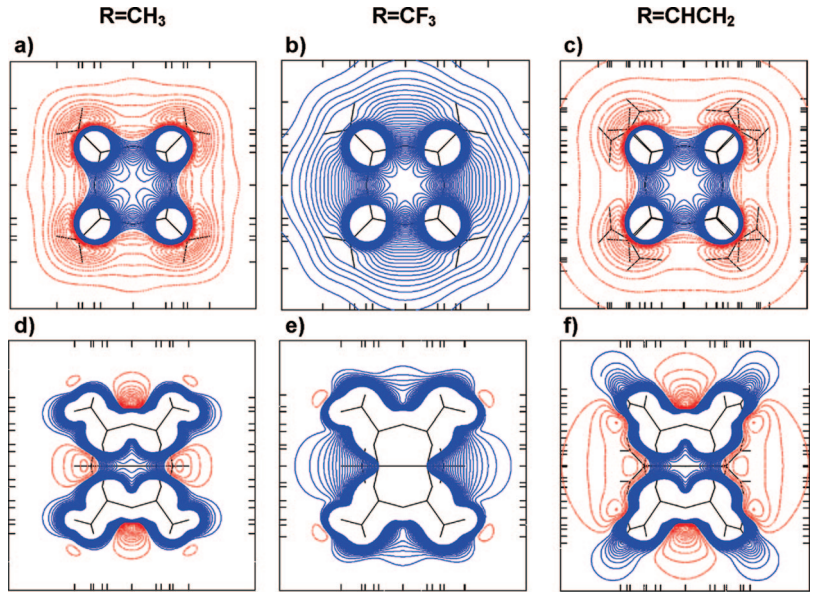

Figure 14. Two-dimensional contour plots of the B3LYP/6-311++G(d,p) molecular electrostatic potentials of R_8T_8 POSS cages; R=CH_3, CF_3, $CHCH_2$. The plotting plane in panels a−c contains the center of the POSS cage and four oxygen atoms, while panels d−f show a diagonal plane through the center of the cage and four silicon atoms. The increment between adjacent contours is 2.5 kcal/(mol-electron) with positive and negative values shown in blue and red, respectively. In panels a−c and d−f, the contours vary from −100.5 to +100.5 and from −80.5 to +80.5 kcal/(mol-electron), respectively. The distance along each axis in plots a−c (d−f) is 12 (16) angstroms.

is not observed because incorporation of a fluoride ion is unfavorable. This is not a thermodynamic effect, as the binding energy of the fluoride is only slightly less for the methyl compared to the vinyl POSS species (−70 vs −77 kcal/mol, respectively, at the MP2/6-311++G(2df)/B3LYP/6-31G* level). The fact that the F^-@$Methyl_8T_8$ species cannot be synthesized suggests that a facile kinetics pathway for F^- insertion is not accessible, perhaps due to the negative charge on the POSS cage.

In order to further examine the substituent effects on the electronic structure of the T_8 cage, the geometries of T_8R_8, with R=CH_3, CH_2=CH, and CF_3 were reoptimized at a higher level of theory (B3LYP/6-311++G(d,p)), with the resulting molecular electrostatic potential (MEP) plots shown in Figure 14. Positive contours, representing susceptibility to nucleophilic attack, are shown in blue. Negative contours, showing susceptibility to electrophilic attack, are shown in red. The positive contour of the R=CF_3 plot shows that this system is particularly susceptible to nucleophilic attack by F^- and is consistent with the large binding energy calculated for both $F^-@(CF_3)_8T_8$ and $F^-@(CF_3CH_2CH_2)_8T_8$. The difference between the R=CH_3 and R=$CHCH_2$ is more subtle and argues for a "kinetic" effect since the binding energies are so similar. The negative contours of R=CH_3 account for the fact that this molecule does not incorporate F^-. The R=$CHCH_2$ plot shows much more diffuse negative contours, probably making attack by F^- more likely in comparison. This interpretation is consistent with the fact that the vinyl species does indeed incorporate fluoride. The vinyl group is apparently efficient in delocalizing electron density away from the cage; the opposite is true for the methyl group. Recent calculations by Kudo and Gordon[84] on the kinetic pathways for POSS cage synthesis highlight the importance of substituents on the silicon atoms for all reaction mechanisms.

F^-@Nonafluorohexyl$_8T_8$. The ESI mass spectrum for the F^-@Nonafluorohexyl$_8T_8$ negative ion has a single peak at 2410 mass units corresponding to the parent ion (Figure 15). The experimental cross section from the ESI ATD is 374 $Å^2$ compared to the calculated cross section of 368 $Å^2$. These results contrast with a recent X-ray crystal structure[44] that

(84) Kudo, T.; Machida, K.; Gordon, M. S. *J. Phys. Chem. A* **2005**, *109*, 5424–5429.

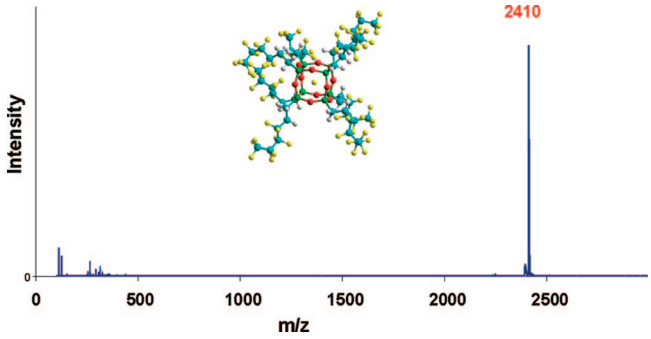

Figure 15. ESI mass spectrum of fluoride species derived from $F^-@[(CF_3(CF_2)_3(CH_2)_2]_8T_8$.

gives a calculated cross section of 350 Å^2. The solid state structure, however, shows a highly ordered parallel arrangement of the fluorohexyl side chains such that each unit resembles a cylinder. This is presumably a solid state packing effect and contrasts with the globular structures predicted by our modeling of the isolated cage system. The ordering in solids has been modeled successfully in long chain perfluoroalkanes and polytetrafluoroethylene, but only by using higher order terms in the molecular dynamics force fields in order to reproduce the observed helical chain structure.[85–87] The POSS cage with capping groups of a similar fluoroalkane, tridecafluorooctyl, did not yield a mass spectrum with enough signal to obtain ion mobility measurements.

Conclusions

In summary, we have succeeded in observing a series of F^-@POSS compounds with assorted capping R-groups. When synthesizing these species, it is essential to restrict the amount of water present to avoid hydrolysis of the cage and the resulting variety of products. The intact cages yield mass spectra in the negative ion ESI and/or the positive ion MALDI experiments. In negative ion ESI studies, the POSS moiety contains a fluoride ion in the center of the cage. DFT calculations show this to be energetically favorable, and the theoretical cross sections of the resulting species agree well with the cross sections of species seen in experiment. In the positive ion MALDI studies, the fluoride ion species is protonated to give either an encapsulated HF (most probable) or a protonated edge oxygen with a sodium ion bound to the outside of the cage. This structure, with HF encapsulated, has been shown to be energetically favorable, and again matches the experimental results. While binding of a lithium ion is more energetically favorable than binding of a sodium ion, the abundance of adventitious sodium ions present under the experimental conditions utilized results in a propensity to form the sodiated species.

The effectiveness of the synthesis of a F^-@POSS molecule depends on the electronic properties of the capping groups. Each of the F^-@POSS species seen in this study has electron-withdrawing capping groups that leave the center of the cage with a positive charge. This charge stabilizes the F^-@POSS structure and also leads to an effective mechanism for F^- encapsulation. If the capping groups are instead electron-donating, such as alkyl groups, the cage has a net negative charge and the formation of a F^-@POSS structure is destabilized. Attempts to encapsulate a fluoride in these cages failed, and reactions with TMAF resulted in no change to the starting structures.

Following the success of trapping fluoride inside POSS molecules, attempts are being made to react TMAF with a variety of POSS oligomers containing electron-withdrawing R-groups under anhydrous synthetic conditions in the hope that one or more cages will incorporate fluoride. Such species should show a strong negative ion ESI spectrum and analogous positive ion MALDI spectra. Incorporation of fluoride into these oligomers should increase the ionization efficiency of these molecules, resulting in stronger molecular ion peaks. It is our hope that this new technique will allow us to study a number of oligomers which have not been accessible in the past.

Acknowledgment. The Air Force Office of Scientific Research under Grants F49620-03-1-0046 and LRIR-92PL0COR is gratefully acknowledged for support of this work. We also thank the NAS/NRC Senior Associateship Program for fellowship support of SEA and the Department of Defense High Performance Computing Modernization Program for grants of computer time at the Engineer Research and Development Center (ERDC) Major Shared Resource Center, Vicksburg, MS.

Supporting Information Available: ^{29}Si and ^{19}F NMR characterization of POSS syntheses data (PDF). This material is available free of charge via the Internet at http: //pubs.acs.org.

CM800058Z

(85) Holt, D. B.; Farmer, B. L. *Polymer* **1999**, *40*, 4667–4672.
(86) Holt, D. B.; Farmer, B. L. *Polymer* **1999**, *40*, 4673–4684.
(87) Borodin, O.; Smith, G. D.; Bedrov, D. *J. Phys. Chem. B* **2002**, *106*, 9912–9922.